PERGAMON

Acta mater. Vol. 47, No. 17, pp. 4375–4386, 1999

Printed in Great Britain
PII: S1359-6454(99)00247-5
1359-6454/99 $20.00 + 0.00

EFFECT OF ELASTIC INTERACTION ON THE FORMATION OF A COMPLEX MULTI-DOMAIN MICROSTRUCTURAL PATTERN DURING A COHERENT HEXAGONAL TO ORTHORHOMBIC TRANSFORMATION

Y. H. WEN[1, 2]†, Y. WANG[2] and L. Q. CHEN[1]

[1]Department of Materials Science and Engineering, The Pennsylvania State University, University Park, PA 16802, U.S.A. and [2]Department of Materials Science and Engineering, The Ohio State University, Columbus, OH 43210, U.S.A.

(Received 9 April 1999; accepted 31 July 1999)

Abstract—The effect of elastic interaction on the formation and dynamic evolution of multi-domain microstructures during a hexagonal to orthorhombic transformation in the absence and presence of an externally applied strain field is investigated numerically using the phase field model. In particular, three cases are considered, which include a single variant, two variants, and all three variants of the orthorhombic phase produced by the transformation. In each case, the morphology and spatial distribution of the orientation variants are characterized. It is shown that nucleation and growth of a single variant produces thin plates of the orthorhombic domains with definite habit planes. In the case of two variants, the domains developed at the initial stages are also platelets of well-defined habit planes, which is similar to the case of a single variant. However, the impingement and intersection of the platelets of different variants results in the formation of twin boundaries and "zig-zag" patterns. The overlap regions of the "zig-zag" cross sections remain untransformed which agrees very well with experimental observations. If all three variants are present, the hexagonal to orthorhombic transformation results in a number of unique multi-domain structures such as the star patterns, compound star patterns, fan patterns, etc., which have been frequently observed experimentally in systems undergoing hexagonal to orthorhombic or similar transformations. It is found that if the boundary of the system is constrained, e.g. a grain embedded in a polycrystalline material, the transformation can go to completion only when all three variants are present. In the presence of external strain field, the coupling between the applied strain field and the stress-free transformation strain associated with the domain formation leads to selective growth of variants. © *1999 Acta Metallurgica Inc. Published by Elsevier Science Ltd. All rights reserved.*

Keywords: Computer simulation; Aging; Phase transformations; Multi-domain microstructure

1. INTRODUCTION

Most advanced engineering materials are inherently heterogeneous. Their microstructure consists of different orientation variants and/or phases. Structural phase transformation is still the most effective way to produce the multi-domain and multi-phase microstructures and hence to control the properties. For example, the hexagonal to orthorhombic transformation observed in many systems [1–9] produces three orientation variants which form very complicated multi-domain morphological patterns. If no external field is applied, all three orientation variants are energetically equivalent and hence have the same probability of appearing during the transformation. The key factor that controls the domain structure and its temporal evolution in this case is the elastic interactions among the internal strain fields associated with different orientation domains. The internal strain fields arise from the lattice accommodation among the parent phase and the orientation variants of the product phase as well as among the orientation variants themselves to maintain the lattice continuity across the interphase and domain boundaries. In the presence of an external field, there is an additional coupling between the external field and the internal strain fields. Such a coupling may change the shape, orientation, volume fraction, and spatial distribution of the variants.

The shape, boundary orientation, spatial arrangement, and relative amount of these orientation domains play an important role in determining the physical and mechanical properties of the material. The main objective of this paper is to understand the effect of the elastic interactions on the formation of the domain structures and their temporal evolution. The phase-field kinetic model is employed for this study, which has proved to be very useful in modeling the mesoscale microstructural evolution during coherent phase transformations [10–13] where the microstructural evolution

†To whom all correspondence should be addressed.

is controlled by the elastic interactions. In this work, we consider a hexagonal to orthorhombic ordering in a prototype two-dimensional model system. The interfaces between the parent and product phases as well as between different orientation domains are assumed to remain coherent during the entire transformation.

2. THE PHASE-FIELD KINETIC MODEL

In the phase-field model, an arbitrary multi-phase and multi-domain microstructure is described by a small set of mesoscopic field variables. For the hexagonal to orthorhombic transformation considered in this paper, for example, the three orientation domains of the orthorhombic phase can be described by three long-range order (lro) parameter fields

$$\eta_1(\mathbf{r}, t), \quad \eta_2(\mathbf{r}, t), \quad \eta_3(\mathbf{r}, t)$$

where t is the time and $\mathbf{r}$ is the spatial coordinate vector. Each of these lro parameter fields characterizes the shape, size, and spatial distribution of one of the three orientation domains. Each lro parameter field assumes a non-zero value within a particular domain and vanishes within the parent phase and other domains. The temporal evolution of these field variables and hence the microstructural evolution are described by the time-dependent Ginzburg–Landau (TDGL) equations [14]

$$\frac{\partial \eta_p(\mathbf{r}, t)}{\partial t} = -L\frac{\delta F}{\delta \eta_p(\mathbf{r}, t)} + \xi_p(\mathbf{r}, t); \quad p = 1, 2, 3 \quad (1)$$

where L is the kinetic coefficient and F is the total free energy of the system, $\delta F/\delta \eta_p(\mathbf{r}, t)$ forms the thermodynamic driving force for the spatial and temporal evolution of η_p, and $\xi_p(\mathbf{r}, t)$ is the Langevin noise term which is taken to be Gaussian distributed and its correlation properties meet the requirements of the fluctuation–dissipation theorem [15]

$$\langle \xi_p(\mathbf{r}, t)\xi_p(\mathbf{r}', t')\rangle = 2k_{\mathrm{B}}TL\delta(\mathbf{r} - \mathbf{r}')\delta(t - t') \quad (2)$$

where k_{B} is the Boltzmann constant. The origin of the noise term is related to the thermal fluctuations of η_p at temperature T.

To numerically solve equation (1), one has to formulate the free energy functional F in terms of the field variables, $\eta_1(\mathbf{r}, t)$, $\eta_2(\mathbf{r}, t)$, and $\eta_3(\mathbf{r}, t)$. In a coherent transformation, the free energy functional consists of the chemical free energy and the elastic strain energy.

2.1. Chemical free energy

The non-equilibrium chemical free energy as a functional of the field variables can be approximated by the conventional Ginzburg–Landau phenomenological formulation [11]. It contains a local specific free energy, $f(\eta_1, \eta_2, \eta_3)$, and non-local gradient terms, i.e.

$$F = \int_V \left[\frac{1}{2}\sum_{p=1}^{3}\lambda_p(\nabla\eta_p)^2 + f(\eta_1, \eta_2, \eta_3)\right] \mathrm{d}V \quad (3)$$

where λ_p are gradient energy coefficients. The integration in equation (3) is carried out over the entire system volume V. As usual, the gradient terms in equation (3) provide an energy penalty to inhomogeneities in the field variables which takes place primarily at interfaces. The local specific free energy $f(\eta_1, \eta_2, \eta_3)$ in equation (3) defines the basic bulk thermodynamic properties of the system and its temperature dependences. It is usually approximated by a Landau-type polynomial expansion following the symmetry operations with respect to the parent phase [9]. The number of allowed terms included in the polynomial usually depends on the nature (e.g. first order or second order) and symmetry change of the transformation as well as the desired accuracy of the local free energy. For the hexagonal → orthorhombic transformation considered in this paper, a general expansion with terms up to sixth order reads

$$\begin{aligned} f(\eta_1, \eta_2, \eta_3) &= \frac{A_2}{2}(T - T_{\mathrm{c}})(\eta_1^2 + \eta_2^2 + \eta_3^2) + \frac{A_3}{3}(\eta_1\eta_2\eta_3) \\ &+ \frac{A_{41}}{4}(\eta_1^4 + \eta_2^4 + \eta_3^4) + \frac{A_{42}}{4}(\eta_1^2\eta_2^2 + \eta_2^2\eta_3^2 \\ &+ \eta_1^2\eta_3^2) + \frac{A_5}{5}(\eta_1\eta_2\eta_3)(\eta_1^2 + \eta_2^2 + \eta_3^2) \\ &+ \frac{A_{61}}{6}(\eta_1^6 + \eta_2^6 + \eta_3^6) + \frac{A_{62}}{6}(\eta_1^4\eta_2^2 + \eta_2^4\eta_3^2 \\ &+ \eta_3^4\eta_1^2) + \frac{A_{63}}{6}(\eta_1^2\eta_2^2\eta_3^2) \end{aligned} \quad (4)$$

where T_{c} is the temperature below which the parent hexagonal loses its stability with respect to the transformation to the orthorhombic phase.

A hexagonal to orthorhombic transformation such as the h.c.p.–B19 order → disorder transformation is thermodynamically first order. Therefore, the coefficient A_{41} should be negative and A_{61} be positive. However, as we pointed out in a recent paper [16], the particular form of the free energy model has no significant effect on the domain structure since it is the competition between the domain wall energy and the elastic strain energy that determines the domain structure after the transformation is completed. Therefore, we employ a simpler three-component order parameter model with fewer expansion coefficients to describe the local free energy density of a homogeneous system in this study, i.e.

$$f(\eta_1,\eta_2,\eta_3)=\frac{1}{2}A_1(T-T_c)(\eta_1^2+\eta_2^2+\eta_3^2)-\frac{1}{4}A_2(\eta_1^4+\eta_2^4+\eta_3^4)+\frac{1}{6}A_3(\eta_1^2+\eta_2^2+\eta_3^2)^3. \quad (5)$$

2.2. Elastic strain energy

Hexagonal → orthorhombic congruent ordering produces strain ε_{ij}^0 in the system. The stress-free strain field is related to ε_{ij}^0 and the lro parameter through

$$\varepsilon_{ij}^0(\mathbf{r})=\sum_{p=1}^{3}\varepsilon_{ij}^0(p)\eta_p^2(\mathbf{r}) \quad (6)$$

where p denotes one of the three orthorhombic variants. The elastic strain is the difference between the total strain and the stress-free strain, i.e.

$$\varepsilon_{ij}^{el}(\mathbf{r})=\varepsilon_{ij}(\mathbf{r})-\varepsilon_{ij}^0(\mathbf{r})=\varepsilon_{ij}(\mathbf{r})-\sum_{p=1}^{3}\varepsilon_{ij}^0(p)\eta_p^2(\mathbf{r}). \quad (7)$$

In the homogeneous modulus approximation, the elastic stress field is related to the elastic strain through

$$\sigma_{ij}(\mathbf{r})=C_{ijkl}\varepsilon_{kl}^{el}(\mathbf{r})=C_{ijkl}\left[\varepsilon_{kl}(\mathbf{r})-\sum_{p=1}^{3}\varepsilon_{kl}^0(p)\eta_p^2(\mathbf{r})\right] \quad (8)$$

where C_{ijkl} is the elastic modulus tensor.

The total elastic energy of the system is given by

$$E_{el}=\frac{1}{2}\int_V\sigma_{ij}(\mathbf{r})\varepsilon_{ij}^{el}(\mathbf{r})\,\mathrm{d}^3(\mathbf{r}). \quad (9)$$

According to Ref. [13], the final form of the total elastic energy of a multi-domain mixture can be expressed as

$$E_{el}=\frac{V}{2}C_{ijkl}\bar{\varepsilon}_{ij}\bar{\varepsilon}_{kl}-VC_{ijkl}\bar{\varepsilon}_{ij}\sum_{p=1}^{3}\varepsilon_{kl}^0(p)\overline{\eta_p^2(\mathbf{r})}+\frac{V}{2}C_{ijkl}\sum_{p=1}^{3}\sum_{q=1}^{3}\varepsilon_{ij}^0(p)\varepsilon_{kl}^0(q)\overline{\eta_p^2(\mathbf{r})\eta_q^2(\mathbf{r})}-\frac{1}{2}\sum_{p=1}^{3}\sum_{q=1}^{3}\int\frac{\mathrm{d}^3\mathbf{g}}{(2\pi)^3}B_{pq}(\mathbf{n})\left\{\eta_p^2(\mathbf{r})\right\}_{\mathbf{g}}^*\left\{\eta_q^2(\mathbf{r})\right\}_{\mathbf{g}}$$

where $\overline{(\ldots)}$ represents the volume average of $(\ldots)$ and V is the total volume of the system. In this work, we limit ourselves to the case that the whole system is subject to a homogeneous applied strain. For this particular case, $\bar{\varepsilon}_{ij}$ is equal to the applied strain ε_{ij}^a [13]. The first term on the right-hand side of the above equation represents the increment of elastic energy related solely to the applied strain/stress. The second term reflects the interaction of the applied strain/stress with the stress-free transformation strain of the product phase which is usually referred to as the mechanical driving force in the context of martensitic transformation [17–19]. The last two terms correspond to the elastic energy generated by an arbitrary structure heterogeneity where $B_{pq}(\mathbf{n})$ is a two-body interaction potential given by

$$B_{pq}(\mathbf{n})=n_i\sigma_{ij}^0(p)\Omega_{jk}(\mathbf{n})\sigma_{kl}^0(q)n_l \quad (11)$$

where $\mathbf{n}=\mathbf{g}/g$ is a unit vector in reciprocal space and n_i is its ith component, $\sigma_{ij}^0(p)=C_{ijkl}\varepsilon_{kl}^0(p)$, and $\Omega_{ij}(\mathbf{n})$ is a Green function tensor which is inverse to the tensor $\Omega_{ij}^{-1}(\mathbf{n})=C_{iklj}n_kn_l$

$$\left\{\eta_q^2(\mathbf{r})\right\}_{\mathbf{g}}=\int\frac{\mathrm{d}^3\mathbf{g}}{(2\pi)^3}\eta_q^2(\mathbf{r})\exp(-\mathrm{i}\mathbf{g}\cdot\mathbf{r})$$

is the Fourier transform of $\eta_q^2(\mathbf{r})$ and $\{\eta_p^2(\mathbf{r})\}_{\mathbf{g}}^*$ is the complex conjugate of $\{\eta_p^2(\mathbf{r})\}_{\mathbf{g}}$.

3. APPLICATION OF THE MODEL TO COHERENT HEXAGONAL TO ORTHORHOMBIC TRANSFORMATIONS

The general stress-free transformation strain tensor for a hexagonal to orthorhombic transformation is given by

$$\varepsilon^0(1)=\begin{pmatrix}a&0&0\\0&b&0\\0&0&c\end{pmatrix}. \quad (12)$$

If we assume that there is no volume change for the transformation and the lattice parameter difference between the hexagonal and orthorhombic phases along the c-direction can be neglected, the transformation strain becomes

$$\varepsilon^0(1)=\varepsilon_s\begin{pmatrix}1&0&0\\0&-1&0\\0&0&0\end{pmatrix} \quad (13)$$

where ε_s represents the magnitude of the shear deformation. The transformation strains for the other two variants can be obtained by symmetry operations, a 120° and a 240° rotation, respectively, which is illustrated in Fig. 1. Therefore, the stress-free strain tensors for all three variants are given by

$$\varepsilon^0(1)=\varepsilon_s\begin{pmatrix}1&0\\0&-1\end{pmatrix},\quad \varepsilon^0(2)=\varepsilon_s\begin{pmatrix}-1/2&\sqrt{3}/2\\\sqrt{3}/2&1/2\end{pmatrix},\quad \varepsilon^0(3)=\varepsilon_s\begin{pmatrix}-1/2&-\sqrt{3}/2\\-\sqrt{3}/2&1/2\end{pmatrix}. \quad (14)$$

With the particular form of the transformation strain given in equations (14), the domain structure evolution during the hexagonal → orthorhombic transformation can be effectively modeled in two dimensions without losing any essential physics.

Assuming that the gradient energy coefficients are independent of the lro parameters, i.e. $\lambda_p=\lambda$, and taking the variational derivative of the chemical

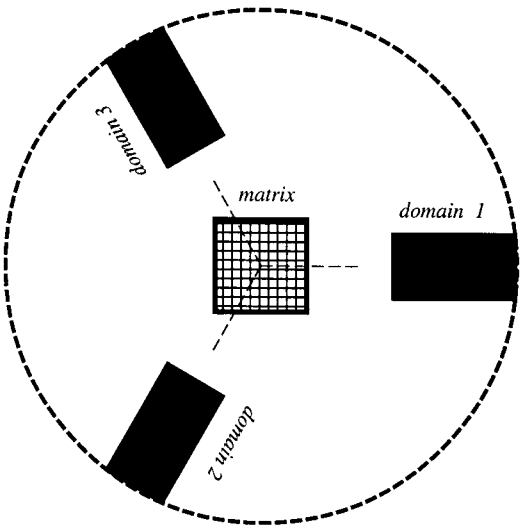

Fig. 1. Relative position of the three domains.

free energy and elastic strain energy with respect to the lro parameters, the field kinetic equation (1) becomes

$$\frac{\partial \eta_p(\mathbf{r}, t)}{\partial t} = -L\left\{ -\lambda\nabla^2(\eta_p(\mathbf{r}, t)) + \frac{\partial f}{\partial \eta_p(\mathbf{r}, t)} + \frac{\delta E_{\mathrm{el}}}{\partial \eta_p(\mathbf{r}, t)} \right\} + \xi_p(\mathbf{r}, t); \quad p = 1, 2, 3$$

where f is defined in equation (5)

$$\frac{\delta E_{\mathrm{el}}}{\delta \eta_p(\mathbf{r}, t)} = 2\eta_p(\mathbf{r}, t)\left[-C_{ijkl}\varepsilon^{\mathrm{a}}_{ij}\varepsilon^0_{kl}(p) + \sum_{q=1}^{3}\left[C_{ijkl}\varepsilon^0_{ij}(p)\varepsilon^0_{kl}(q)\eta^2_q(\mathbf{r}, t) - \left\{ B_{pq}(\mathbf{n})\left\{\eta^2_q(\mathbf{r}, t)\right\}_{\mathbf{g}}\right\}_{\mathbf{r}}\right]\right]$$

where $\{B_{pq}(\mathbf{n})\{\eta^2_q(\mathbf{r}, t)\}_{\mathbf{g}}\}_{\mathbf{r}}$ is the inverse Fourier transform of $B_{pq}(\mathbf{n})\{\eta^2_q(\mathbf{r}, t)\}_{\mathbf{g}}$. The readers are referred to Refs [12, 13] for more details.

Assuming that the system is elastically isotropic (on the basal plane of a hexagonal lattice, the elastic constants are indeed isotropic) the Green function in equation (11) becomes

$$\Omega_{ij}(\mathbf{n}) = \frac{\delta_{ij}}{G} - \frac{n_i n_j}{2G(1-\nu)} \tag{17}$$

where G is the shear modulus and ν is Poisson's ratio of the material under investigation. Substituting equation (17) into equation (11) and using equations (14) in the definition of $\sigma^0_{ij}(p) = C_{ijkl}\varepsilon^0_{kl}(p)$ gives

$$B_{pq}(\mathbf{n}) = 4Gn_i\varepsilon^0_{ij}(p)\varepsilon^0_{jl}(q)n_l - 2G\frac{1}{1-\nu}[n_i\varepsilon^0_{ij}(p)n_j][n_k\varepsilon^0_{kl}(q)n_l]. \tag{18}$$

Substituting the transformation strains (14) into equation (18), we have

$$B_{pq}(\mathbf{n}) = 2G\varepsilon_{\mathrm{s}}^2\left(3\delta_{ij} - 1 - \frac{1}{1-\nu}I(p)I(q)\right) \tag{19}$$

where δ_{ij} is the Kronecker-delta function and

$$I(p) = \left(n_1^2 - n_2^2,\ -\frac{n_1^2}{2} + \frac{n_2^2}{2} + \sqrt{3}n_1n_2,\ -\frac{n_1^2}{2} + \frac{n_2^2}{2} - \sqrt{3}n_1n_2\right). \tag{20}$$

The diagonal terms of B_{pq} represent the self energies of the three orientation variants and the off-diagonal terms represent the interactions between the variants. In principle, if we assume the interfacial energy of the domain boundaries to be isotropic, their orientations can be determined from the elastic energy minimization. The coefficient $G\varepsilon_{\mathrm{s}}^2$ in equation (19) defines the typical elastic energy of the system. It has been used in the simulation as a normalization factor. The shear magnitude ε_{s} is used as the unit to define the externally applied strain.

Before the numerical simulation, the kinetic equations should be presented in their dimensionless forms. Following the same line as in Ref. [12], we have introduced a reduced time, defined as $\tau = L|\Delta f|$, and reduced spatial coordinates, defined as $u_i = x_i/l$. In these definitions, $|\Delta f|$ is the free energy difference between the hexagonal and orthorhombic phases (it is a driving force for the transformation at the aging temperature), and l is the length scale assigned to the computational grid increment. Substituting these reduced variables into equations (15) and (16), we get the dimensionless form of the kinetic equation:

$$\frac{\partial \eta_p(\mathbf{u}, \tau)}{\partial \tau} = -\left\{ -\beta\nabla^2(\eta_p(\mathbf{u}, \tau)) + \frac{\partial f_{\mathrm{a}}}{\partial \eta_p(\mathbf{u}, \tau)} + \alpha\frac{\delta E'_{\mathrm{el}}}{\delta \eta_p(\mathbf{u}, \tau)}\right\} + \xi'_p(\mathbf{u}, t) \tag{21}$$

where

$$\alpha = \frac{4G\varepsilon_{\mathrm{s}}^2}{|\Delta f|}, \quad \beta = \frac{\lambda}{l^2|\Delta f|}$$

$$f_{\mathrm{a}} = \frac{1}{2}a_1(\eta_1^2 + \eta_2^2 + \eta_3^2) - \frac{1}{4}a_2(\eta_1^4 + \eta_2^4 + \eta_3^4) + \frac{1}{6}a_3(\eta_1^2 + \eta_2^2 + \eta_3^2)^3 \tag{22}$$

with

$$a_1 = \frac{A_1}{|\Delta f|}, \quad a_2 = \frac{A_2}{|\Delta f|}, \quad a_3 = \frac{A_3}{|\Delta f|}$$

and

$$\frac{\delta E'_{\mathrm{el}}}{\delta \eta_p(\mathbf{u}, \tau)} = \frac{2\eta_p(\mathbf{u}, \tau)}{4G\varepsilon_s^2}\Bigg[- C_{ijkl}\varepsilon_{ij}^{\mathrm{a}}\varepsilon_{kl}^{0}(p) + \sum_{q=1}^{3}\Bigg[C_{ijkl}\varepsilon_{ij}^{0}(p)\varepsilon_{kl}^{0}(q)\eta_q^2(\mathbf{u}, \tau) - \Big\{ B_{pq}(\mathbf{n})\Big\{\eta_q^2(\mathbf{u}, \tau)\Big\}_{\mathbf{g}'}\Big\}_{\mathbf{u}}\Bigg]\Bigg]$$

where

$$\mathbf{g}' = \mathbf{g}l,$$

$$\langle \xi_p'(\mathbf{u}, \tau)\xi_p(\mathbf{u}', \tau')\rangle = \frac{2k_{\mathrm{B}}T}{|\Delta f|l^3}\delta(\mathbf{u} - \mathbf{u}')\delta(\tau - \tau').$$

To solve equation (21), the dimensionless parameters α, β, a_1, a_2, and a_3 need to be specified. α and β characterize the ratio of strain energy and interfacial energy vs chemical driving force. They are assumed to be 15.0 and 0.1, respectively, in this simulation. The parameters a_1, a_2, and a_3 define the chemical free energy. These polynomial expansion coefficients in our phenomenological chemical free energy functional have been chosen in such a way that it provides a qualitatively correct geometry of the free energy surface, e.g. with triple degenerated global minima at $(\eta_1 = 1, \eta_2 = 0, \eta_3 = 0)$, $(\eta_1 = 0, \eta_2 = 1, \eta_3 = 0)$, and $(\eta_1 = 0, \eta_2 = 0, \eta_3 = 1)$, which correspond to each of the three orientation variants of the orthorhombic phase, and a local minimum at $(\eta_1 = 0, \eta_2 = 0, \eta_3 = 0)$, which corresponds to the parent hexagonal phase. The following values have been used in this work: $a_1 = 1.82$, $a_2 = 19.7$, and $a_3 = 18.0$. The normalized chemical free energy for one single domain is illustrated in Fig. 2.

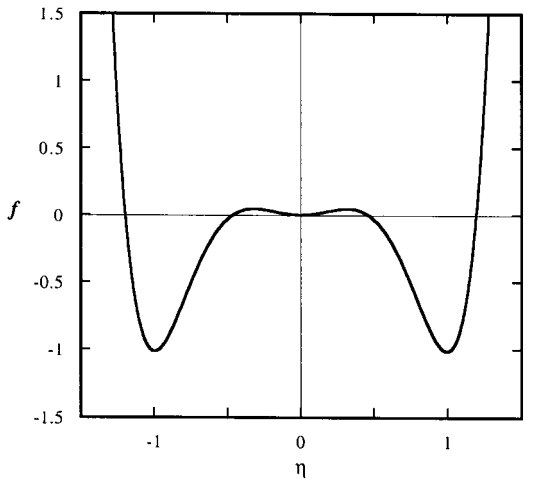

Fig. 2. The specific free energy as a function of the lro parameter.

4. RESULTS AND DISCUSSION

Equation (21) is solved numerically in reciprocal space using a semi-explicit algorithm [20]. The system size is 1024×1024 grid points for all the simulations. Periodical boundary conditions are applied along both dimensions. All the simulations start from a homogeneous hexagonal phase characterized by $\eta_1 = \eta_2 = \eta_3 = 0$, which is metastable according to Fig. 2. The nucleation process of the stable orthorhombic phase is described by the Langevin noise terms in the equation. After a certain number of nuclei have been generated, the noise terms are switched off and the microstructural evolution is controlled by growth and coarsening of the nuclei.

4.1. Nucleation and growth of the orthorhombic phase in a single-variant system

The main concern here is the habit plane orientation of a single domain. This can be determined from the elastic energy minimization. As can be seen from the elastic energy expression in equation (10), the first three terms on the right-hand side are independent of the microscopic arrangement of the structural pattern and they are either a function of applied fields or a function of the total amount of the transformed domain. The last term containing B_{pq} is, however, microstructure-dependent. The energy will be minimized when $B_{pq}(\mathbf{n})$ reaches its maximum. The three single domains should be aligned along the orientations with maximized $B_{11}(\mathbf{n})$, $B_{22}(\mathbf{n})$, $B_{33}(\mathbf{n})$, respectively. This requires that $(I(1))^2$, $(I(2))^2$, and $(I(3))^2$ be minimum considering the expression of $B_{pq}(\mathbf{n})$ in equation (19). Taking the expression of $I(p)$ in equation (20) and substituting n_1 and n_2 with $\cos(\theta)$ and $\sin(\theta)$, respectively, one has

$$(I(p))^2 = (\cos^2(2\theta), \cos^2(2\theta + 60), \cos^2(2\theta - 60)). \tag{23}$$

Minimization of $(I(1))^2$, $(I(2))^2$, and $(I(3))^2$ with respect to θ leads to the habit plane orientations for each variant:

$$\theta(\text{domain 1}) = \pm 45^\circ, \quad \theta(\text{domain 2}) = \begin{cases} 15^\circ \\ -75^\circ \end{cases}, \quad \theta(\text{domain 3}) = \begin{cases} 75^\circ \\ -15^\circ \end{cases}. \tag{24}$$

Each variant has two identical orthogonal domains. The predicted habit plane orientations for the three domains are illustrated in Fig. 3. The domain structure of the three variants obtained from the computer simulation is shown in Fig. 4. The white regions

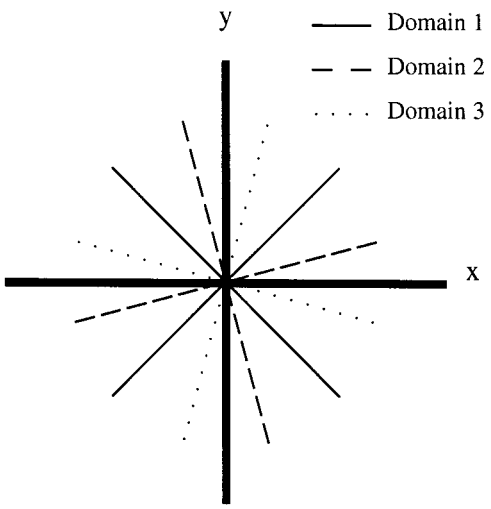

Fig. 3. Schema of predicted habit plane normals.

represent the orthorhombic phase while the black areas represent the parent hexagonal phase. Figures 4(a)–(c) show the particle morphologies of the three variants of the orthorhombic phase formed at an early stage of nucleation and growth ($\tau = 30$) while Figs 4(d)–(f) correspond to a later stage ($\tau = 1000$). At all stages, the orthorhombic phase particles assume a thin plate morphology along the predicated habit plane orientations. At earlier stages of the transformation, more plates are present. Further aging leads to domain growth and coarsening, resulting in fewer plates ($\tau = 1000$).

It should be pointed out that the orthorhombic precipitates and the hexagonal matrix in Fig. 4 have the same composition. Since the chemical free energy of the orthorhombic phase is lower than the hexagonal phase (see, e.g. Fig. 2), the entire system is expected to transform to the orthorhombic phase. The fact that the transformation from the hexagonal phase to the orthorhombic phase cannot go to completion reveals the importance of the elastic energy contribution to phase equilibria. Similar results were also obtained in the phase field simulation of martensitic transformations [12]. As a result of the elastic energy contribution which is roughly proportional to the precipitate volume, a two-phase equilibrium can be established even in a single-phase system. The amount of transformed orthorhombic phase will increase when the system is quenched to a lower temperature as the chemical driving force increases.

4.2. Morphological evolution of a two-variant system

Figure 5 shows the simulated morphological evolution in the presence of variants 1 and 2. The bright, dark, and gray areas represent variant 1, variant 2, and the hexagonal matrix, respectively. Figure 5(a) shows the nucleated orthorhombic par-

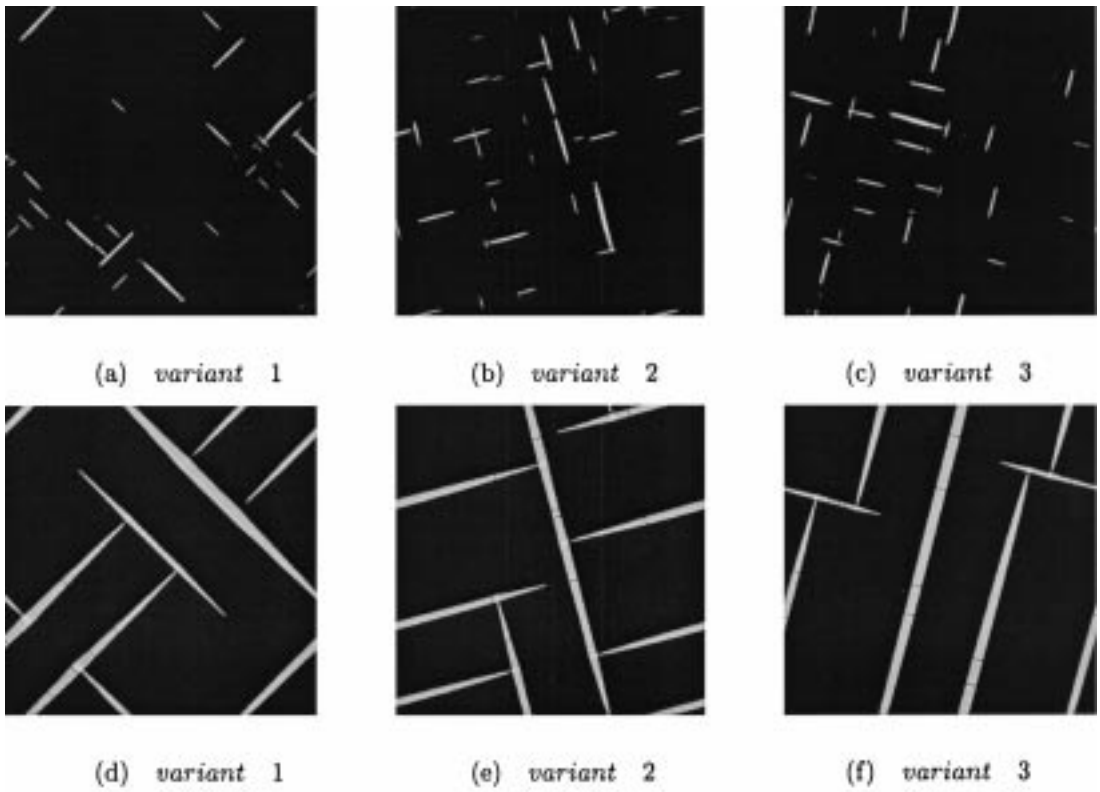

Fig. 4. Morphology of domains for the three variants of the orthorhombic phase at two different stages when they exist alone: (a)–(c) are at $\tau = 30$ and (d)–(f) at $\tau = 1000$.

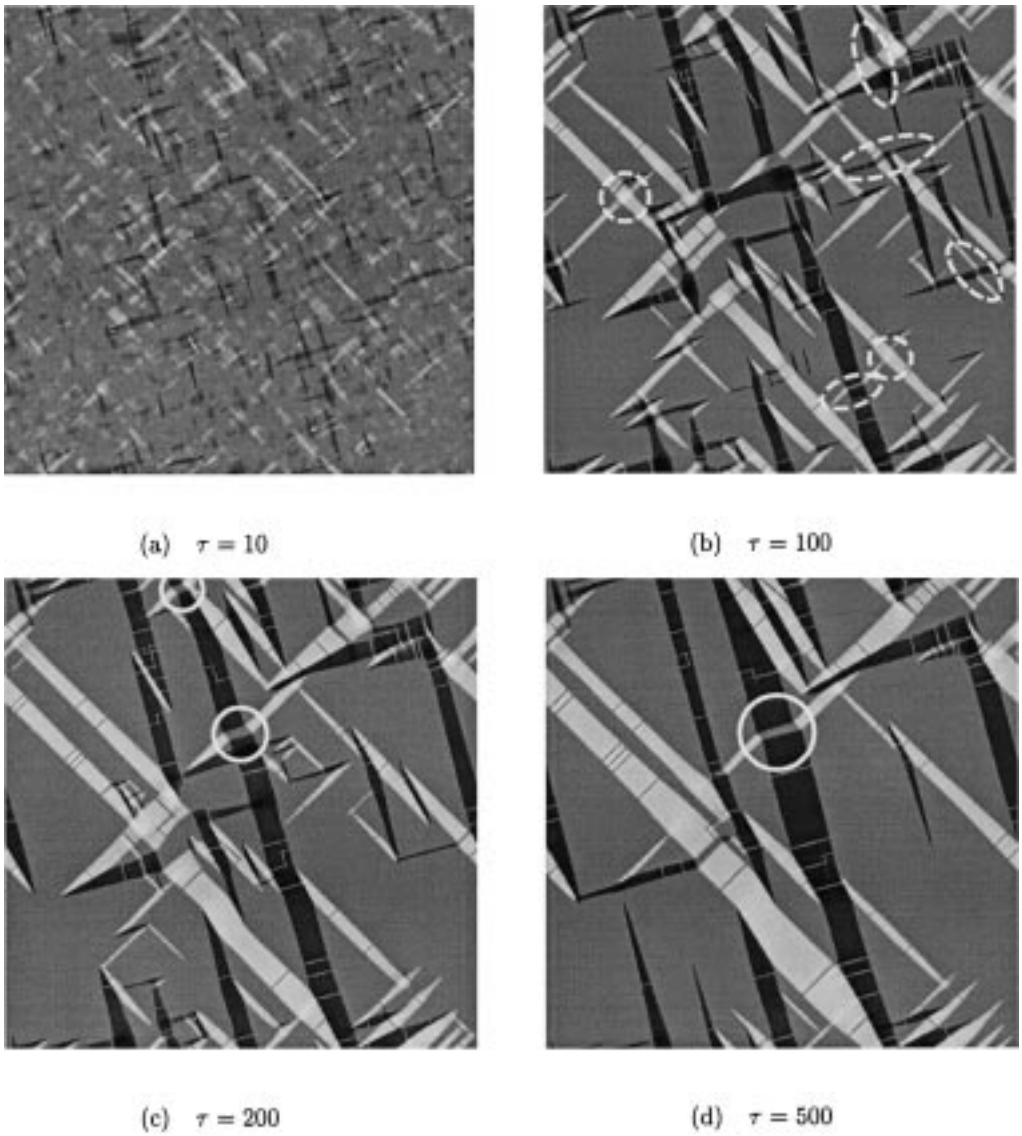

Fig. 5. Morphology evolution with two domains transforming concurrently.

ticles at $\tau = 10$. Domains of both variants grow along their respective habit orientations as shown in the previous section (refer to Fig. 4). Their morphology is mainly thin plate, similar to the single-variant system discussed above. However, when the domains of different orientation variant intersect, interesting "zig-zag" configurations are formed [refer to those areas in Fig. 5(b) highlighted by dashed circles and ellipsoids, respectively]. It is interesting to note that the overlapping regions of two different variants retain the parent phase symmetry [refer to areas enclosed by the solid circles in Figs 5(c) and (d)]. This phenomenon was observed experimentally by Yang and Wayman during the intersecting of two ε-martensite variants in Fe–Mn–Si shape memory alloy (see fig. 4 in Ref. [21]). The transformation of h.c.p. ε-martensite from the f.c.c. matrix is accomplished by a shear which is the same as in our case.

Coarsening of the domain structure results in the disappearance of small platelets and growth of large ones, leaving the total amount of the orthorhombic phase unchanged. Similar to the single-variant system, the hexagonal to orthorhombic transformation cannot go to completion as a result of the elastic energy contribution.

4.3. Morphological evolution in a three-variant system

For the three-variant system, we use different shades of gray, i.e. bright, gray, and dark, to represent variants 1, 2, and 3, respectively. Similar to the single- and two-variant systems, the transformation starts from nucleation and growth of the

orthorhombic domains from the hexagonal matrix, followed by domain coarsening. Details of the domain evolution process for this three-variant system without external fields have been presented in a previous publication [16].

The focus here is on the effect of mutual lattice accommodation among the orientation variants on the domain patterns by comparing the three-variant system with the single- and two-variant systems. In contrast to the single- and two-variant systems, the hexagonal to orthorhombic transformation in the three-variant system can readily go to completion. It can be shown that the bulk elastic energy can be essentially reduced to zero by a mixture of three variants whose transformation strains are described by equations (14). With equal volume fraction of 1/3 for each variant, the average transformation strain ($\bar{\varepsilon}$) within a volume element whose volume is much larger than the typical domain size, is given by

$$\bar{\varepsilon} = \frac{1}{3}\varepsilon^0(1) + \frac{1}{3}\varepsilon^0(2) + \frac{1}{3}\varepsilon^0(3) = \frac{1}{3}\varepsilon_s \begin{pmatrix} 1 & 0 \\ 0 & -1 \end{pmatrix} + \frac{1}{3}\varepsilon_s \begin{pmatrix} -1/2 & \sqrt{3}/2 \\ \sqrt{3}/2 & 1/2 \end{pmatrix} + \frac{1}{3}\varepsilon_s \begin{pmatrix} -1/2 & -\sqrt{3}/2 \\ -\sqrt{3}/2 & 1/2 \end{pmatrix}. \quad (25)$$

It turns out that the average transformation strain vanishes within a mixture of three variants of equal fraction. This is impossible in single- and two-variant systems.

As a result of the elastic energy accommodation, most of the orthorhombic domains in the three-variant system adopt different morphologies as compared to the previous cases. As shown in Fig. 6, by the time $\tau = 20$ [Fig. 6(a)], essentially the entire system has transformed into a single orthorhombic phase with a mixture of three orientation variants of roughly equal volume fractions. The domain structure after significant coarsening is shown in Fig. 6(b). There are a lot of interesting complex multi-domain patterns resulting from the elastic energy accommodation. For example, we can find a number of star patterns as highlighted by circles in Fig. 6(b). There are also compound stars formed by the combination of two single stars [indicated by ellipsoids in Fig. 6(b)]. These morphological patterns are very similar to the experimentally observed ones [see Fig. 7(b)]. The joint of a star structure with a fan-like one (enclosed by a dotted square) also shows remarkable agreement with experimental observations [refer to Fig. 7(c)]. Moreover, there is a perfect star pattern (refer to the area enclosed by a square in the lower left) which is exactly the same as shown in Fig. 7(b).

The system size of our simulations can be estimated by fitting the specific domain boundary energy calculated from the computer simulation to the corresponding experimental value. In order to compare the domain size obtained by our simulation [Fig. 6(b)] with those observed by experiments as shown in Fig. 7, we need to find specific domain boundary energy γ, the shear modulus G, and the shear magnitude ε_s for lead orthovanadate crystal. Unfortunately, we could not locate these data in the literature. If we take γ to be 200 mJ/m^2, the same as the interfacial energy in γ-TiAl [22], and use the shear modulus $G = 46.15$ GPa for TiAlNb [23], and assume the shear magnitude ε_s to be 0.03 [24], then the grid increment l is estimated to be 5×10^{-8} cm [16]. Based on this estimation, the system size is approximately 0.5 μm ($1024 \times l$).

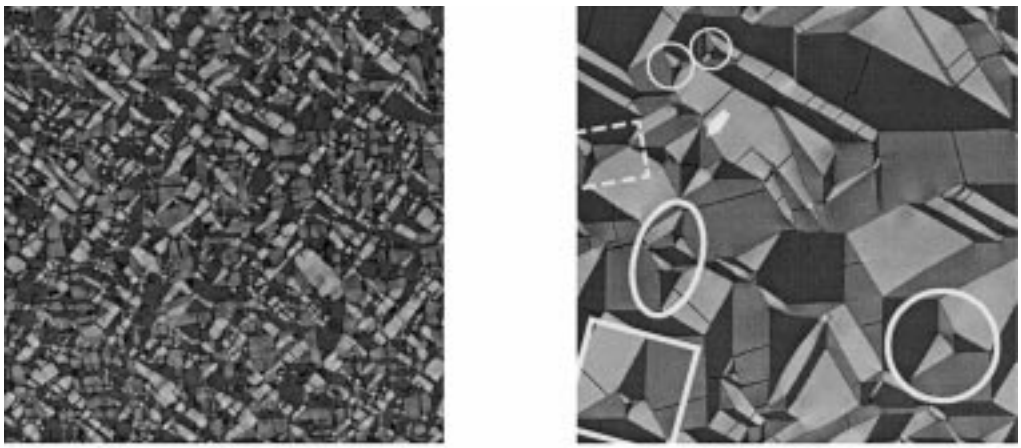

Fig. 6. Temporal microstructural evolution during nucleation and growth of orthorhombic domains from a hexagonal matrix obtained using the phase-field model with 1024×1024 grid points: (a) $\tau = 20$; (b) $\tau = 5000$.

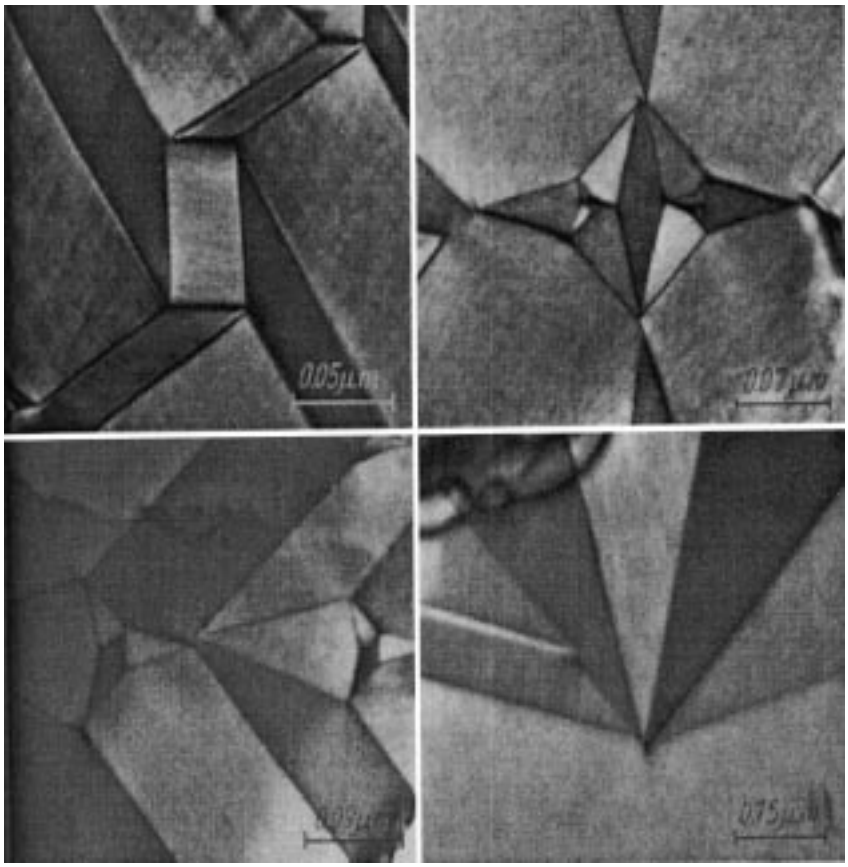

Fig. 7. Characteristic orientation domain configurations observed during hexagonal → monoclinic transformations by Manolikas and Amelinckx [8] (with permission from the publisher to include it here).

Getting back to the simulated morphology shown in Fig. 6(b), the length scale of the star pattern enclosed by a white square in the lower left is roughly 1/6 of the system size which corresponds to a size of 0.08 μm. This value agrees very well with that observed experimentally in Fig. 7(b).

4.4. Influence of externally applied strain

All the domain structures presented so far are free from external fields. When an external field (strain in our case) is applied, the coupling between the applied strain and the stress-free transformation strain of domains could strongly affect the microstructural evolution. This effect is reflected by the coupling term, $-VC_{ijkl}\overline{\varepsilon_{ij}}\sum_{p=1}^{3}\varepsilon_{kl}^{0}(p)\overline{\eta_p^2(\mathbf{r})}$ in equation (10). Since the three variants have different stress-free transformation strains in the global frame coordinate as expressed in equations (14), this coupling term has different values for different variants and thus promotes or depresses the growth of certain orientation domains. As a result, the growth of the domains becomes selective.

For simplicity, we applied a uniaxial strain to investigate its influence on the microstructural evolution. The external strain is applied along such a direction that variants 1 and 2 are equally favored while variant 3 is unfavored. Such a strain is given by

$$\varepsilon^{\text{applied}} = \varepsilon^{\text{amp}}\begin{pmatrix} 3/4 & \sqrt{3}/4 \\ \sqrt{3}/4 & 1/4 \end{pmatrix} \tag{26}$$

where ε^{amp} is the amount of applied strain given in the unit of the shear magnitude of the stress-free transformation strain, ε_s in equations (14). Three different magnitudes of the applied strain, i.e. $0.1\varepsilon_s$, $0.25\varepsilon_s$, and $1.0\varepsilon_s$, respectively, are considered.

In Fig. 8, we show the influence of an applied strain field on the morphological evolution in a three-variant system. We use the same shades of gray to represent different orientation variants of the orthorhombic phase as described in the previous section, i.e. bright, gray, and dark represent variants 1, 2, and 3, respectively. Figures 8(a)–(c) show the domain evolution under a relatively small applied strain with a magnitude of $0.1\varepsilon_s$. Figures 8(d)–(f) correspond to a moderate applied strain with magnitude of $0.25\varepsilon_s$, and the last three micrographs in Fig. 8 correspond to a high applied strain with a magnitude of $1.0\varepsilon_s$. Microstructures developed at three different times, i.e. $\tau = 50$, 100, and 500, are presented for the three cases.

As can be seen from Figs 8(a)–(c), the domain structures are more or less similar to the case without an externally applied strain. The effect of the

applied strain on the shapes and mutual arrangement of domains is not significant when the magnitude of the applied strain is small. For example, one can still find the star structure in Fig. 8(c) (highlighted by a solid circle), compound star structure (enclosed by a solid ellipsoid), swastika-symbol-like structure (enclosed by a solid squares), and fan-pattern structure (enclosed by a dashed ellipsoid), etc.

When the applied strain becomes larger ($0.25\varepsilon_s$) [Figs 8(d)–(f)], the situation changes. During the early stages of the aging process [Fig. 8(d)], for example, only domains of variants 1 (bright) and 2 (dark) which are favored by the externally applied strain nucleate and grow. Domains of variant 3 are absent. This implies that the externally applied strain results in a selective nucleation and growth of domains of variants 1 and 2. The mutual arrange-

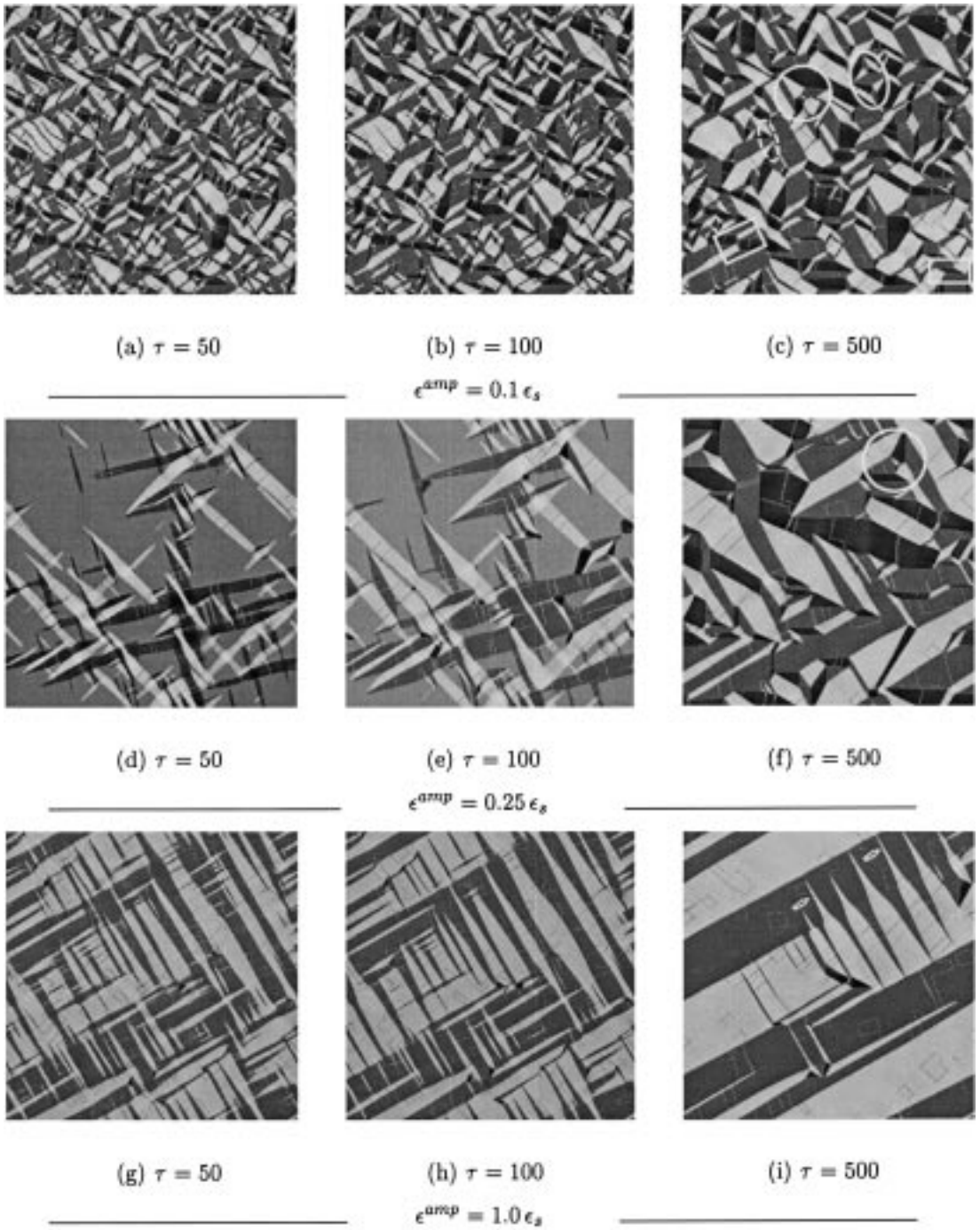

Fig. 8. Influence of different amount of applied strains on the temporal domain evolution.

ment of these domains is similar to the two-variant system without an externally applied strain as presented in Fig. 5. Also the spatial arrangement of domains (relative angles among the plates) is similar [compare the results shown in Fig. 8(d) with those in Fig. 5(b)]. However, at a later time, domain 3 (black) appeared as shown in Fig. 8(e). This is an indication that the internal strain (or stress) accumulated because the absence of domain 3 becomes increasingly important as the domains of variants 1 and 2 grow. As a result, further aging leads to a significant increase in the volume fraction of variant 3. However, its total amount is still much less than those of variants 1 and 2 in the final stage as shown in Fig. 8(f). In some local area, one can even find a star pattern accompanying the appearance of all the three variants [highlighted by a solid circle in Fig. 8(f)].

When the applied strain is further increased to be of the same magnitude as the shear deformation ($1.0\varepsilon_s$) [Figs 8(g)–(i)], the resultant domain structure consists of predominantly domains of variants 1 and 2 during the entire evolution process which means the applied strain plays a dominant role in the whole process. The two domains show some preferred orientations, approximately 30° or 120° relative to the *x*-axis of the system, in order to well accommodate their transformation strains. Such a structure pattern agrees very well with those observed experimentally during a $DO_{19} \rightarrow$ O-phase transformation by Bendersky (see results shown in figs 3 and 7 in Ref. [25]). In explaining why it has predominantly two orientation domains, he argued one possible reason might be due to the effect of quenched stresses. Our numerical results can lend support to his reasoning.

In Fig. 8(i), it is interesting to note some sharp tips at the end of some domains approaching an intersection with some other domains (indicated by white open arrows) in an effort to minimize corresponding elastic energy. This kind of domain morphology is quite common and has been observed in different materials. For instance, in TiAlNb alloy by Bendersky [24], $Pb_3(PO_4)_2$ by J. Torres and $YBa_2Cu_3O_7$ superconductor (see fig. 7.17 in Ref. [26]), etc.

5. SUMMARY

The formation and temporal evolution of domain structures during a hexagonal to orthorhombic transformation is studied using a phase-field model. The focus has been on the effect of elastic interactions on the domain formation and evolution during nucleation, growth, and coarsening. It is shown that the elastic interactions among the orientation variants of the orthorhombic phase are critical in controlling the domain morphology. In order to demonstrate the importance of mutual accommodation among the three variants, we examined the domain pattern evolution during the transformation of the hexagonal phase into a single variant, two variants, and three variants of the orthorhombic phase. With the same chemical driving force and the same magnitude of the transformation strain, the phase transformation for the single- and two-variant systems cannot go to completion, resulting in a stable two-phase mixture with plate-shaped orthorhombic precipitates coherently embedded in the hexagonal matrix, whereas the transformation can readily go to completion in the three-variant system, resulting in a single orthorhombic phase with the three variants forming complex domain patterns. The domain patterns obtained from the simulations show excellent agreement with existing experimental observations on systems undergoing hexagonal to orthorhombic or to monoclinic transformations.

We also investigated the effect of an applied strain field on the domain structure development. We show that the domain evolution depends on the magnitude and direction of the applied load. A relatively low applied strain (compared to the magnitude of the transformation strain for domain formation) has no significant influence on the domain structure. A moderate applied strain results in a selective nucleation of only two orthorhombic variants in the initial stages of transformation. The third variant appears at later times when the internal strain/stress accumulated with the selective growth of two variants becomes comparable with the effect due to the externally applied strain. A high applied strain results in a strongly orientated domain structure. In order to avoid direct intersection with another approaching domain and thus avoid a high interaction energy, some sharp tips emerge at the end of domains. This phenomenon was commonly observed in different materials with orientation domains.

Acknowledgements—We are grateful for the financial support by ONR under grant number N00014-95-1-0577 (Wen and Chen), DMR-96-33719 (Chen), and NSF under grant DMR-9703044 (Wen and Wang). The simulation was performed at the San Diego Supercomputer Center and the Pittsburgh Supercomputing Center.

REFERENCES

1. Igonin, G. S., Makogon, M. B. and Igonina, T. N., *Fizika Metall. Metalloved.*, 1970, **30**, 543.
2. Igonin, G. S., Makogon, M. B. and Igonina, T. N., *Fizika Metall. Metalloved.*, 1970, **30**, 727.
3. Vicens, J. and Delavignette, P., *Physica status solidi* (a), 1976, **33,** 497.
4. Sinclair, R. and Dutkiewicz, J., *Acta metall.*, 1977, **25**, 235.
5. Bendersky, L. A. and Boettinger, W. J., *J. Res. Natn. Inst. Stand. Technol.*, 1993, **98**, 585.
6. Kitano, Y. and Kifune, K., *Ultramicroscopy*, 1991, **39**, 279.

7. Kitano, Y., Kifune, K. and Komura, Y., *J. Physique, Colloque C*, 1988, **5**, 201.
8. Manolikas, C. and Amelinckx, S., *Physica status solidi* (a), 1980, **60,** 607.
9. Izyumov, Yu. A. and Syromyatnikov, V. N., *Phase Transitions and Crystal Symmetry, Fundamental Theories of Physics*. Kluwer Academic, New York, 1990.
10. Wang, Y., Chen, L. and Khachaturyan, A., in *Solid–Solid Phase Transformations*, ed. W. C. Johnson, J. M. Howe, D. E. Laughlin and W. A. Soffa. The Minerals, Metals and Materials Society, Warrendale, PA, 1994, p. 245.
11. Khachaturyan, A. G., *Theory of Structural Transformations in Solids*. John Wiley, New York, 1983.
12. Wang, Y. and Khachaturyan, A. G., *Acta mater*., 1997, **45**, 759.
13. Li, D. Y. and Chen, L. Q., *Acta mater*., 1998, **46**, 639.
14. Gunton, J. D., Miguel, M. S. and Sahni, P. S., in *Phase Transitions and Critical Phenomena*, Vol. 8, ed. C. Domb and J. L. Lebowith. Academic Press, New York, 1983, pp. 267–466.
15. Lifshitz, E. M. and Pitaevskii, L. P., *Statistical Physics*. Pergamon Press, Oxford, 1980.
16. Wen, Y. H., Wang, Y. Z. and Chen, L. Q., *Phil. Mag. A*, in press.
17. Ganghoffer, J. F., Denis, S., Gautier, E., Simon, A. and Sjostrom, S., *Eur. J. Mech. A*, 1993, **12**, 21.
18. Wen, Y. H., Denis, S. and Gautier, E., *J. Physique IV, Colloque C2*, 1995, **5**, 531.
19. Wen, Y. H., Denis, S. and Gautier, E., *J. Physique IV, Colloque C1*, 1996, **6**, 475.
20. Chen, L. Q. and Shen, J., *Comput. Phys. Commun*., 1998, **108**, 147.
21. Yang, J. H. and Wayman, C. M., *Acta metall. mater*., 1992, **40**, 2011.
22. Rao, S., Woodward, C. and Hassledine, P. M., *Mater. Res. Soc. Symp. Proc*., 1994, **319**, 285.
23. Boyer, R., Welsch, G. and Collings, E. W., *Materials Properties Handbook, Titanium Alloys*. ASM International, Materials Park, OH, 1994.
24. Bendersky, L. A., Private communication, 1998.
25. Bendersky, L. A., *Scripta metall*., 1993, **29**, 1645.
26. Salje, E. K. H., *Phase Transitions in Ferroelastic and Co-elastic Crystals*. Cambridge University Press, Cambridge, 1993.